JACS
JOURNAL OF THE AMERICAN CHEMICAL SOCIETY
pubs.acs.org/JACS
Article

Exploring Cuneanes as Potential Benzene Isosteres and Energetic Materials: Scope and Mechanistic Investigations into Regioselective Rearrangements from Cubanes

Jeong-Yu Son,[#] Santeri Aikonen,[#] Nathan Morgan, Alexander S. Harmata, Jesse J. Sabatini, Rosario C. Sausa, Edward F. C. Byrd, Daniel H. Ess,* Robert S. Paton,* and Corey R. J. Stephenson*

Cite This: *J. Am. Chem. Soc.* 2023, 145, 16355−16364

ABSTRACT: Cuneane is a strained hydrocarbon that can be accessed via metal-catalyzed isomerization of cubane. The carbon atoms of cuneane define a polyhedron of the C_{2v} point group with six faces—two triangular, two quadrilateral, and two pentagonal. The rigidity, strain, and unique exit vectors of the cuneane skeleton make it a potential scaffold of interest for the synthesis of functional small molecules and materials. However, the limited previous synthetic efforts toward cuneanes have focused on monosubstituted or redundantly substituted systems such as permethylated, perfluorinated, and bis(hydroxymethylated) cuneanes. Such compounds, particularly rotationally symmetric redundantly substituted cuneanes, have limited potential as building blocks for the synthesis of complex molecules. Reliable, predictable, and selective syntheses of polysubstituted cuneanes bearing more complex substitution patterns would facilitate the study of this ring system in myriad applications. Herein, we report the regioselective, Ag^{I}-catalyzed isomerization of asymmetrically 1,4-disubstituted cubanes to cuneanes. In-depth DFT calculations provide a charge-controlled regioselectivity model, and direct dynamics simulations indicate that the nonclassical carbocation invoked is short-lived and dynamic effects augment the charge model.

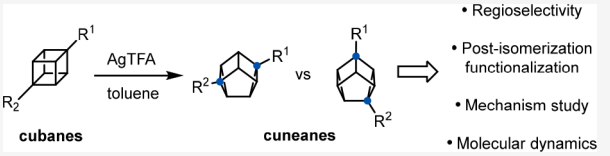

INTRODUCTION

Cubane has continuously inspired the chemical community since its synthesis was first reported by Eaton in 1964 due, in large part, to its beautiful symmetry, high strain energy, and impressive kinetic stability.[1] Consequently, cubane derivatives have been studied in a multitude of applications ranging from energetic materials to pharmaceuticals (Figure 1A).[2] Decades after publishing his seminal cubane synthesis, Eaton noted the similar exit vectors of 1,4-disubstituted cubanes and *para*-disubstituted benzene rings, leading him to propose cubane as a potential scaffold for drug development.[3] This hypothesis has stimulated further research comparing the performance and properties of benzene-derived and cubane-derived functional molecules in both biological and abiotic systems.[4,5]

For all the attention cubane has received, relatively little has been given to its aliphatic hydrocarbon isomer, cuneane, despite its potential as a valuable molecular scaffold in its own right (Figure 1A).[6] The synthesis of cuneane was first reported by Eaton in 1970 and was achieved via the Ag^{I}- or Pd^{II}-catalyzed isomerization of cubane (Figure 1B).[7] Beyond preparing the parent compound, Eaton demonstrated the rearrangement with several mono- and *symmetrically* 1,4-disubstituted cubanes (Figure 1B and Figure 1C, respectively). The former gave mixtures of all three possible cuneane isomers, while the latter gave only two (of ten possible) substitution patterns (hereafter the "1,3- and 2,6-isomers"). Eaton attributed the selectivity for the 1,3- and 2,6-isomers over the eight other possible substitution patterns to the reaction's progression "via the most economic bond-switching path." The relative amounts of 1,3- vs 2,6-isomer product formed were highly substituent-dependent.

No significant advances in the synthesis of cuneanes were made for the following 50 years, despite researchers revisiting the related Rh-catalyzed valence isomerization of cubanes to cyclooctatetraenes, which was also reported by Eaton in 1970.[8] However, during the preparation of this manuscript, Matsubara and co-workers reported the synthesis of enantioenriched, redundantly 2,6-substituted cuneanes using asymmetric silver and (preferentially) palladium catalysts.[9] The same manuscript describes the racemic Ag^{I}-catalyzed isomerization of 2 *asymmetrically* 1,4-disubstituted cubanes to 2,6-disubstituted cuneanes, the first such examples in the literature.

In the course of ongoing work involving the alkylation of cubane derivatives, we serendipitously observed the highly regioselective rearrangement of an *asymmetrically* 1,4-disubstituted cubane to one of the corresponding 1,3-cuneane

Received: March 28, 2023
Published: July 24, 2023

https://doi.org/10.1021/jacs.3c03226
J. Am. Chem. Soc. 2023, 145, 16355−16364

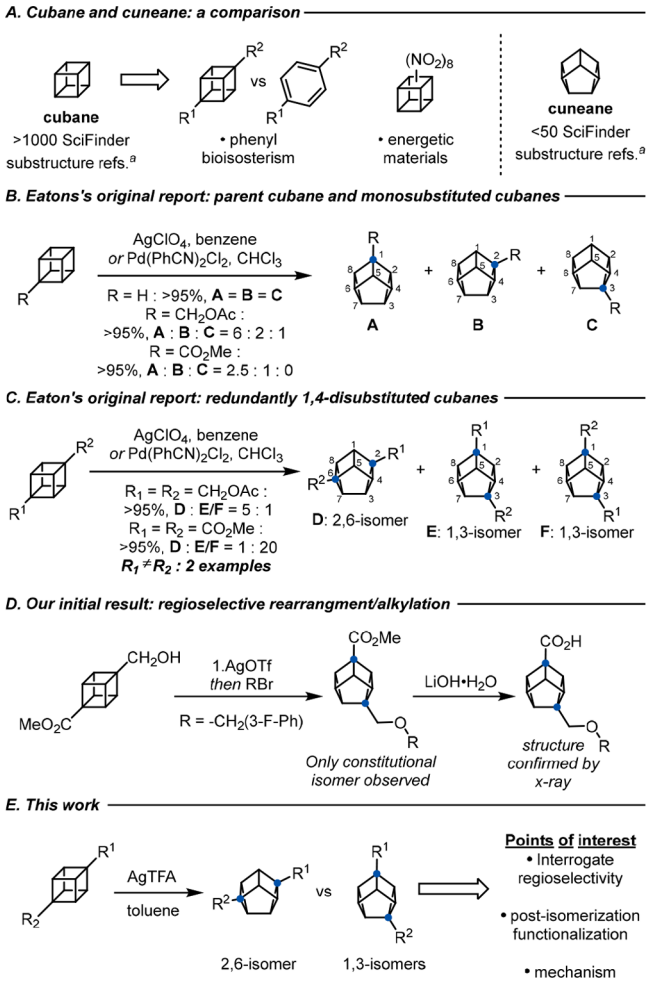

Figure 1. Background on the limited chemistry of cuneanes. [a]Reference counts were made on the basis of SciFinder[n] substructure searches conducted on 05/17/2023.

isomers (Figure 1D). The value of this regioselectivity was immediately apparent as an entry point to a range of differentially 1,3-disubstituted cuneanes. We were surprised to find no literature precedent at the time for the rearrangement of such asymmetrically disubstituted substrates. We entered the study described herein to develop the scope of this transformation and determine key substituent effects on regioselectivity. Furthermore, we hoped to gain a mechanistic understanding of the basis of the observed selectivity.

RESULTS AND DISCUSSION

1a was selected as the optimization substrate, as it is commercially available and would directly lead to a cuneane bearing a synthetically versatile carboxylic acid functional handle. We examined the isomerization of cubane **1a** as the model substrate by using a variety of Ag^I catalysts in toluene at 80 °C (Table 1, entries 1−5). While the reaction proceeds slowly under these conditions, higher temperatures were avoided due to safety considerations based on suspected exothermic decomposition of cuneanes supported by differential scanning calorimetry of purified samples (see Supporting Information (SI)). The regioselective isomerization occurred with 1 equiv of AgTFA, providing desired cuneane in 70% yield (2,6- to 1,3-isomer ratio = 13:1) (Table 1, entry 5). Many silver catalysts and the intermediates of ring-strained isomer-

Table 1. Reaction Optimization

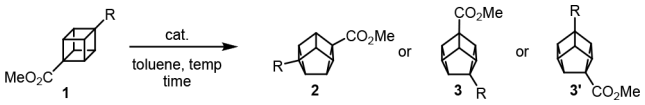

entry	cat. (1 equiv)	R	temp (°C)	yield (2:3:3′)(%)[a]
1	$AgBF_4$	CO_2H	80	5:0:0
2	$AgPF_6$	CO_2H	80	30:0:0
3	AgOAc	CO_2H	80	0:0:0
4	AgOTf	CO_2H	80	48:0:0
5	AgTFA	CO_2H	80	65:5 (3 + 3′)
6[b]	**AgTFA**	**CO_2H**	**80**	85:5 (3 + 3′) (75)[c,d]
7	$PdCl_2$	CO_2H	80	42:5 (3 + 3′)
8	$BF_3{\cdot}Et_2O$	CO_2H	80	0:0:0
9	TFA	CO_2H	80	0:0:0
10[b]	AgTFA (0.3)	CO_2H	80	30:0:0
11[b]	AgTFA	CO_2H	60	40:0:0
12[b]	AgTFA	CH_2OH	40	0:99:0
13[b]	**AgTFA (0.5)**	**CH_2OH**	**40**	**0:99:0**[d]

[a]Reaction conditions: **1** (0.1 mmol, 1.0 equiv) and catalyst (1.0 equiv) were reacted in toluene (1.0 mL) for 15 h. NMR yield using CH_2Br_2 as an internal standard. [b]Without light. [c]After recrystallization, only the isomer **2** was obtained. [d]Isolated yield.

ization are sensitive to light. When this reaction was carried out without light, the yield was slightly increased with a 2,6- to 1,3-isomer ratio of 17:1 (Table 1, entry 6). The pure 2,6-cuneane compound could be isolated in 75% yield, following recrystallization. Replacing AgTFA with Pd catalysts gave diminished yields, while replacing it with Lewis acids or TFA (trifluoroacetic acid) led to no product formation (Table 1, entries 7−9). The loading of catalyst and reaction temperature were then examined. When **1a** was reacted with a substoichiometric amount of AgTFA or at 60 °C, cuneane was produced in 30% and 40% yields, respectively, after the 15 h reaction time (Table 1, entries 10 and 11). Further attempts at lower catalyst loading for the isomerization of **1a** demonstrated that turnover does occur but too slowly to be practical (see Supporting Information). Thus, the conditions of entry 6 were deemed satisfactory. We next looked into the isomerization of **1f**, as this was implicated in our original serendipitous result (Figure 1D). Indeed, we found that **1f** isomerizes to give 1,3-isomer **3f** with excellent selectivity, with only traces of other constitutional isomers detected by crude ^1H NMR analysis. In contrast to **1a**, **1f** isomerizes efficiently at mild temperature (40 °C) and under substoichiometric AgTFA (0.5 equiv) conditions (Table 1, entry 13). While further reduction of the catalyst loading was tolerated for **1f** (see Supporting Information), the drastic difference in reactivity between **1a** and **1f** led us to employ high-AgTFA, forcing conditions in the subsequent regioselectivity study to ensure the timely achievement of complete conversion without substrate-specific optimizations. Given the apparent stability of cuneanes to prolonged AgTFA exposure and the low value of inexpensive AgTFA relative to functionalized cubanes, we found this was a reasonable trade-off.

Next, we explored the scope and regioselectivity of the isomerization using a range of asymmetrically and symmetrically 1,4-disubstituted cubanes. Cubanes bearing two electron-withdrawing groups generally rearranged in high yields to the 2,6-isomer with moderate to good selectivity. Reaction of 1-

https://doi.org/10.1021/jacs.3c03226
J. Am. Chem. Soc. 2023, 145, 16355−16364

acid-4-methyl ester (**1a**), 1,4-dimethyl ester (**1b**), and 1-cyano-4-*N*,*N*-diisopropyl amide (**1d**) cubanes gave excellent selectivity for the 2,6-isomers **2a**, **2b**, and **2d**, respectively, in good yields (Table 2). Furthermore, the potentially sensitive

Table 2. Reaction Scope Study

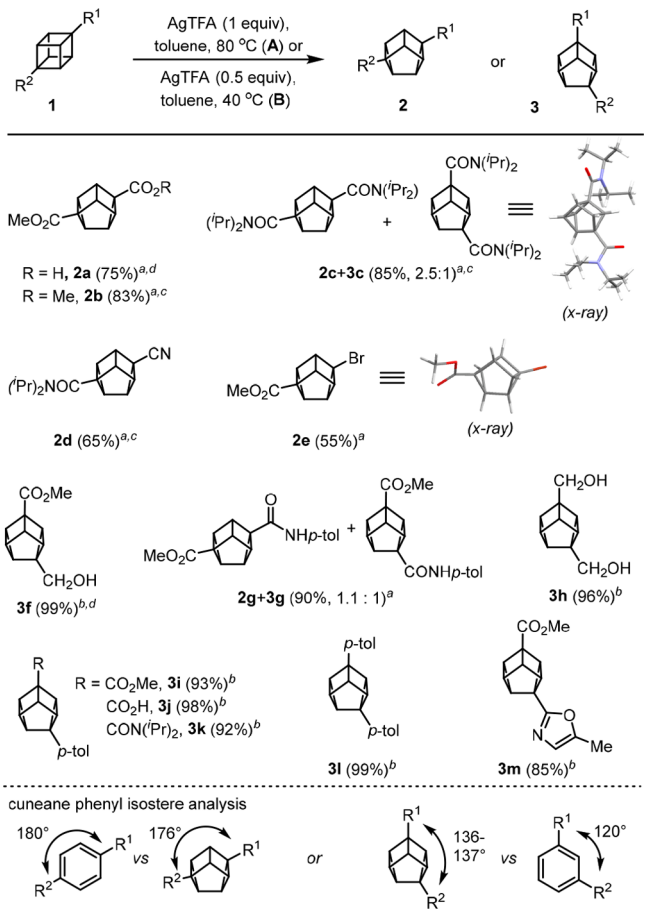

[a]Condition A: **1** (0.1 mmol, 1.0 equiv), AgTFA (1.0 equiv), and toluene (0.1 M) were reacted at 80 °C in amber vial for 15 h. Isolated yield. [b]Condition B: **1** (0.1 mmol, 1.0 equiv), AgTFA (0.5 equiv), and toluene (0.1 M) were reacted at 40 °C in amber vial for 15 h. [c]Reaction for 30 h. [d]5 mmol scale.

bromide group of **2e** was also tolerated. However, 1,4-diamide (**1c**) and 1-amide-4-methylester (**1g**) cubanes underwent rearrangement in good yield with poor regioselectivity. When cubanes bearing one electron-withdrawing and one electron-donating group were treated with AgTFA, single 1,3-isomers were produced in moderate to excellent yields. 1-Methylester-4-hydroxymethyl (**1f**) and 1,4-dihydroxymethyl (**1h**) cubanes underwent rearrangement in 99% and 96% yields, respectively, providing 1,3-cuneanes **3f** and **3h**. Cubanes possessing one electron-withdrawing group and the *p*-tolyl moiety on the opposite vertex were gratifyingly compatible with the reaction conditions, generating **3i**–**3k** in 92–98% yields. Similarly, the rearrangement of a diaryl cubane (**1l**) took place efficiently in this reaction system to furnish **3l** in a quantitative yield. A heteroaryl substituted cubane was easily converted to the corresponding cuneane **3m** and obtained in 85% yield. Furthermore, this protocol was also compatible on a large scale; conducting the rearrangement with 5 mmol of **1a** and **1f** afforded the corresponding cuneanes **2a** and **3f** in 75% and 99% yields, respectively.

Crystallographic analysis of **3j** and **3c** shows a 136°–137° angle between the exit vectors defined by the bonds between the cage and the 1- and 3-substituents, which is comparable to the ∼120° exit vector angle of *meta*-disubstituted arenes. In contrast, crystallographic analysis of **2e** shows a 176° angle between the exit vectors defined by the bonds between the cage and the 2- and 6-substituents, which is comparable to the ∼180° exit vector angle of *para*-disubstituted arenes. While saturated isosteres of *para*-disubstituted arenes abound in the literature, fewer reports have described mimicry of *meta*-disubstituted arenes by saturated systems.[10] The 1,3-disubstituted cuneane scaffold may prove to be a valuable complement to such systems in the development of pharmaceuticals and other functional materials.

To establish the synthetic value of functionalized cuneanes accessible via Ag-catalyzed rearrangement, we explored a variety of subsequent functional group manipulations. Compound **3a** emerged as a potentially useful synthetic intermediate to target in our study. "Half-esters" of alkyl diacids serve as common, useful building blocks for the preparation of differentially disubstituted sp^3-rich scaffolds.[10] Indeed, commercially available cubane **1a** served as a convenient starting material for our substrate scope study. While **2a** could serve as a general precursor to 2,6-disubstituted cuneanes, previously unknown compound **3a** could serve the same role as 1,3-disubstituted cuneanes (Figure 2A). Several

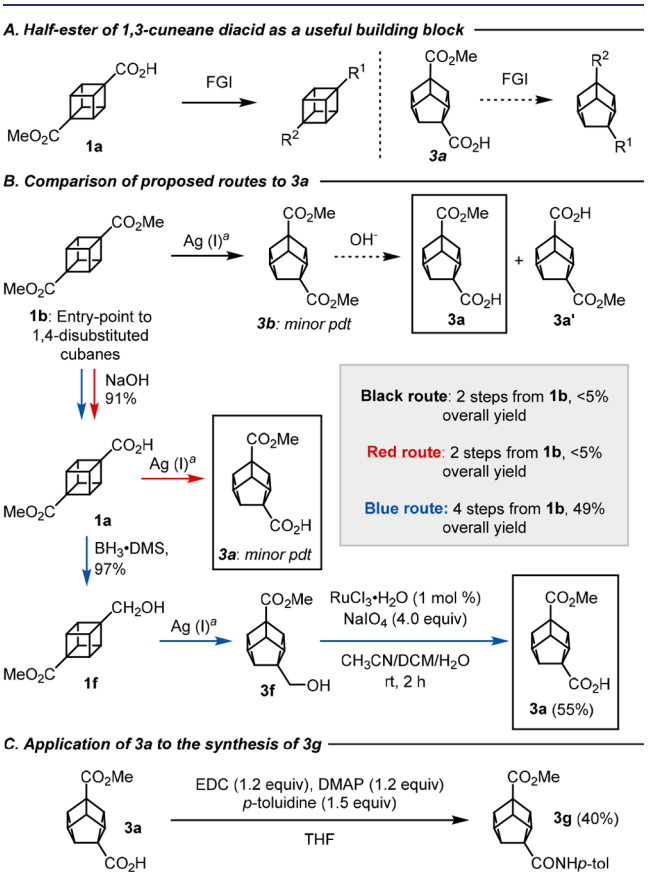

Figure 2. Building blocks are accessed via oxidation and reduction. [a]See Table 2 for yield and selectivity data. FGI = functional group interconversions.

https://doi.org/10.1021/jacs.3c03226
J. Am. Chem. Soc. 2023, 145, 16355–16364

possible routes to **3a** were considered (Figure 2B). Compared with the proposed black and red routes, the route shown in blue is efficient; the regioselective rearrangement of **1f** to **3f** more than compensates for its requisite oxidation state manipulations.

Given the value of amines as building blocks for medicinal chemistry and the apparent incompatibility of carbamates with the reaction conditions, we aimed to install nitrogenous functionality on a preformed cuneane. Curtius rearrangement of **2a** provided isolable carbamate **2n** in high yield (Figure 3,

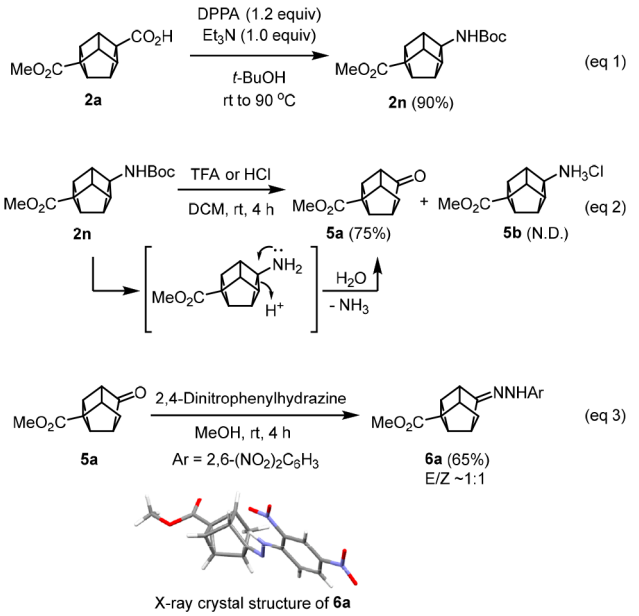

Figure 3. Curtius rearrangement and hydrolysis.

eq 1). Exposure of **2n** to acids failed to yield amine hydrochloride **5b**, but instead afforded ketone **5a** in 90% yield (Figure 3, eq 2), the structure of which was determined via single-crystal X-ray diffraction analysis of its dinitrophenylhydrazone (Figure 3, eq 3). Similar ketone-forming reactivity is precedented with other strained-ring amines such as bicyclo[2.2.0]hexan-1-amine.[11] Cubylamines are also prone to ring-opening, though their hydrochloride salts are generally isolable.[3]

Further experiments were conducted to compare the reactivities of cubane and cuneane congeners. For instance, we were able to repeat Itami's recent work demonstrating the *ortho*-lithiation/zincate formation and Negishi coupling of cubanes.[12] However, subjecting **2d** to the same conditions showed no desired reactivity and decomposition of the starting material (Figure 4, eq 1). Gratifyingly, nickel-promoted decarboxylative arylation of **2o** gave a 54% yield of **2i** with an electron-poor, substituted bipyridine ligand system (Figure 4, eq 2).[13] Cuneane **2i** is notably inaccessible via direct rearrangement of the corresponding cubane **1i**, which exclusively gives 1,3-disubstituted cuneane **3i** upon exposure to AgTFA (vide supra).

To gain insight into the thermal stability of cuneanes and to identify potential safety hazards, we evaluated the thermal decomposition behavior of several cuneanes by differential scanning calorimetry (DSC; see Supporting Information for details and DSC traces). 2,6-Disubstituted cuneane **2a** showed an exotherm with an extrapolated onset temperature of 212 °C

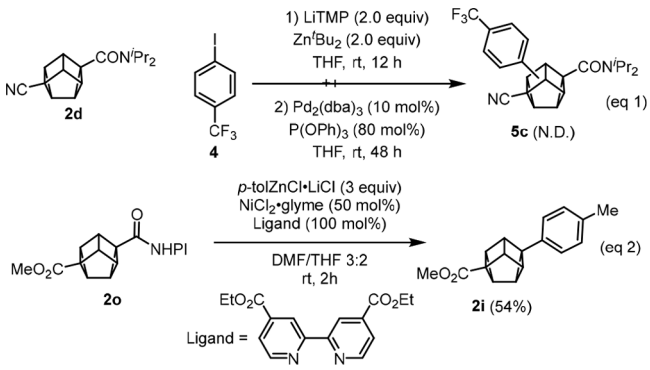

Figure 4. Arylation of cuneane skeleton; NHPI = phthalimide *N*-oxyl group.

and a left-limit onset (T_{init}) of between 170 and 180 °C. This is comparable to the corresponding cubane **1a**, which showed an exotherm immediately following a sharp endotherm at 187 °C. The exotherms experienced by **1a** and **2a** occur well above the 80 °C reaction conditions for Ag-promoted isomerization of **1a** to **2a** and the boiling point of toluene (111 °C), the reaction solvent. In contrast, the T_{init} for exothermic decomposition of **3a** occurs near 120 °C. However, as **3a** is a trace component of the mixture produced upon Ag-promoted isomerization of **1a** at 80 °C, and **3a** is generated from **3f** at room temperature, we do not consider the relatively low T_{init} for **3a** to be cause for concern for processes reported herein. Building block **3f** itself showed a dramatic exotherm with T_{init} at approximately 100 °C, lower than that observed for the corresponding cubane **1f**.

In addition to the carboxylic acid and alcohol building blocks described above, cubane amide **1g** and corresponding cuneanes **2g** and **3g** were evaluated by DSC as these compounds are representative of the "fragment"-sized synthetic intermediates that might be encountered on a medicinal chemistry campaign. Each showed exotherms with T_{init} greater than 150 °C. However, as in the **1a**, **2a**, and **3a** carboxylic acid series, the 1,3-disubstituted cuneane **3g** experienced an exotherm at lower temperature than the corresponding 2,6-disubstituted cuneane or cubane. The related arylated cuneane **2i** likewise decomposed with a T_{init} greater than 150 °C, well above the temperature required for its synthesis from **2o** (23 °C).

While DSC data alone is insufficient for a complete hazard analysis, these results suggest that 1,3- and 2,6-substituted cuneanes are thermally stable at the temperature of typical organic reactions (<100 °C) but are nonetheless prone to exothermic decomposition initiated at temperatures readily achieved in the laboratory (<200 °C). We have not directly observed a hazardous cuneane decomposition event, but we recommend that chemists interested in synthesizing, manipulating, or functionalizing cuneanes perform such operations on small scale with minimal heating and conduct a thoughtful hazard analysis in accordance with institutional policies on potentially energetic materials before proceeding with scale-up.

We also sought to compare the energetic properties of nitrated cubane and cuneane derivatives, specifically nitrate esters **5d**, **5e**, and **5f** (Figure 5). The 2,6-cuneane **2h**, inaccessible by direct isomerization, was prepared by reduction of **2a** and was obtained in 75% yield (Figure 5, eq 1). Frustratingly, attempts at nitration of **2h** and **3h** using the relatively mild nitrating agent acetyl nitrate led only to unproductive decomposition to complex mixtures, which

https://doi.org/10.1021/jacs.3c03226
J. Am. Chem. Soc. 2023, 145, 16355−16364

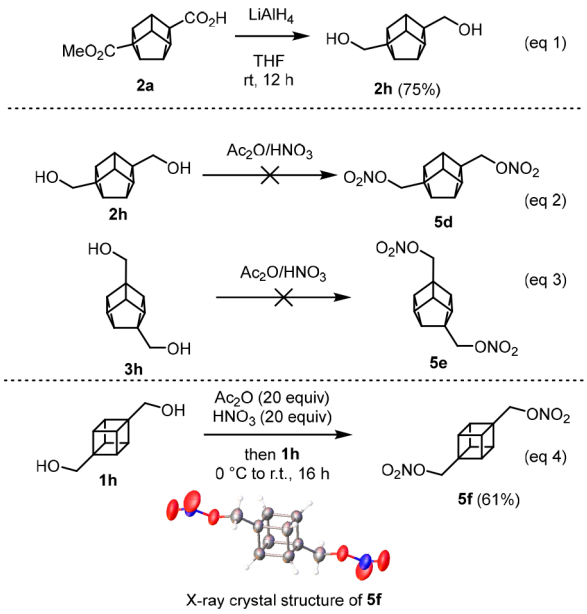

Figure 5. Efforts toward cubane and cuneane nitrate esters.

presented as low-energy gums, suggesting inadvertent destruction of the cuneane skeleton (Figure 5, eqs 2−3). However, cubane **1h** was successfully nitrated using acetyl nitrate to give previously reported nitrate ester **5f** (Figure 5, eq 4).[14−18] The isolation process required modification to provide a sufficiently pure material for analysis. We found that trituration of the gummy, impure concentrate of the dichloromethane extract using ethyl acetate gave pure **5f** as a white, crystalline solid. While this nitration procedure and isolation proved robust and scalable, attempted nitration of **1h** with chilled nitric acid led to spontaneous ignition (hypergolic behavior).

The energetic properties of **5f** were determined through a combination of experimental and computational techniques (Table 3). Differential scanning calorimetry showed a sharp, exothermic decomposition of **5f** beginning at 141 °C, somewhat higher than the reported decomposition temperature of 123−124 °C.[15] No melting was observed prior to decomposition. Impact and friction sensitivities were determined according to the NATO STANAG guidelines.[19,20] The density of 1.516 g/cm^3, determined using single crystal X-ray diffraction crystallography, is comparable to the previously reported value of 1.512 g/cm^{-3}.[15]

Table 3. Physical and Energetic Properties of Dinitratomethyl Cubane 5f

Data category	Dinitratomethyl cubane
T_{dec} [°C][a]	141.0
Ω_{CO2} [%][b]	−119.7
Ω_{CO} [%][c]	−56.7
ρ [g cm^{-3}][d]	1.516
P_{cj} [GPa][e]	17.2
V_{det} [ms^{-1}][f]	7116
I_{sp} [s][g]	224.8
$\Delta_f H°$ [kJ mol^{-1}][h]	244.9
IS[i] [J]	7.0
FS[j] [N]	156
ESD[k] [J]	0.125

[a]T_{dec} = onset temperature of decomposition. [b]Ω_{CO2} = CO_2 oxygen balance. [c]Ω_{CO} = CO oxygen balance. [d]ρ = experimentally determined density. [e]P_{cj} = detonation pressure. [f]V_{det} = detonation velocity. [g]I_{sp} = specific impulse. [h]$\Delta_f H°$ = molar enthalpy of formation. [i]IS = impact sensitivity. [j]FS = friction sensitivity. [k]ESD = electrostatic discharge sensitivity.

Computations were performed to study the isomerization reaction mechanism and origins of regioselectivity by combining static and dynamic trajectory calculations. Density functional theory (DFT) calculations were carried out with TURBOMOLE 7.3[21] and ORCA 4.2.1.[22] Conformer sampling was done using xTB,[23] CREST,[24] and CENSO[25] program packages. Geometry optimizations and vibrational frequencies were calculated using the dispersion corrected hybrid functional PBE0-D3(0)[26,27] with the def2-TZVP[28] basis set since PBE0 gives good geometries for transition metal complexes.[29−31] Final gas-phase single-point energy calculations were carried out with random phase approximation (RPA)[32] using PBE0/def2-QZVPP orbitals. Solvation effects for toluene were accounted for using COSMO[33−35] for geometries and frequencies and COSMO-RS[33,36−38] for single-point energies. Additionally, we used Grimme's quasi-RRHO approximation.[39] Gas-phase Born−Oppenheimer molecular dynamics (BOMD) trajectory calculations were initialized and propagated in Gaussian 16[40] with energies and gradients evaluated at the PBE0-D3/def2-TZVP level of theory. Full computational details are presented in the SI.

In the experiment, substrate-dependent selectivity for either 1,3- or 2,6-cuneanes was observed. To rationalize these observations, we first studied the isomerization mechanism of **1b** since it gave 2,6-cuneane **2b** as the major product and 1,3-cuneane **3b** as a minor product. While the kinetics of related isomerization reactions have been studied,[41,42] to the best of our knowledge, computational mechanistic studies of the cubane to cuneane isomerization have not been previously reported. Our calculations reveal a reactive potential energy surface (PES) that is highly complex: distinct mechanistic pathways converge to form the same regioisomeric product, the identity of the rate-limiting TS varies across pathways, and there is a presence of nonclassical carbocationic intermediates. Further, we employed direct dynamic calculations to study selectivity of branching points that were skipped on the static PES.

A recent review concluded that the reactive silver(I) salt can be either mononuclear or binuclear, although the distinction is difficult to make.[43] We considered the reactive Ag(I) species as mononuclear. Accounting for the homolytic dissociation of the Ag(I) dimer is challenging and will affect the absolute free energies for the whole PES. Here, we use half of the dimer energy as the reference state for AgTFA. The isomerization of **1b** is initiated by Ag(I) insertion to one of the cubane's two inequivalent C−C bonds: C1−C2 (**TS1**$_{C1-C2}$) or C2−C2 (**TS1**$_{C2-C2}$) (Figure 6a). This is the first branching point in the mechanism: C2−C2 insertion ultimately leads toward a single product (**2b**), whereas the regiochemical outcome (**2b** vs **3b**) of C1−C2 insertion is decided at the next step.

Addition to the C2−C2 bond had an activation free energy barrier of 26.8 kcal·mol^{-1} and was favored over C1−C2 addition by 3.2 kcal·mol^{-1}. In the bridged C2−Ag−C2 intermediate (**Int-2**$_{C2-C2}$) formed in this first step, one of the equivalent Ag−C2 bonds can break heterolytically. This barrier constitutes the turnover determining step for the major (C2−C2, **2b**) pathway at 28.2 kcal·mol^{-1} (**TS2**$_{C2Ag-C2}$). The

https://doi.org/10.1021/jacs.3c03226
J. Am. Chem. Soc. 2023, 145, 16355−16364

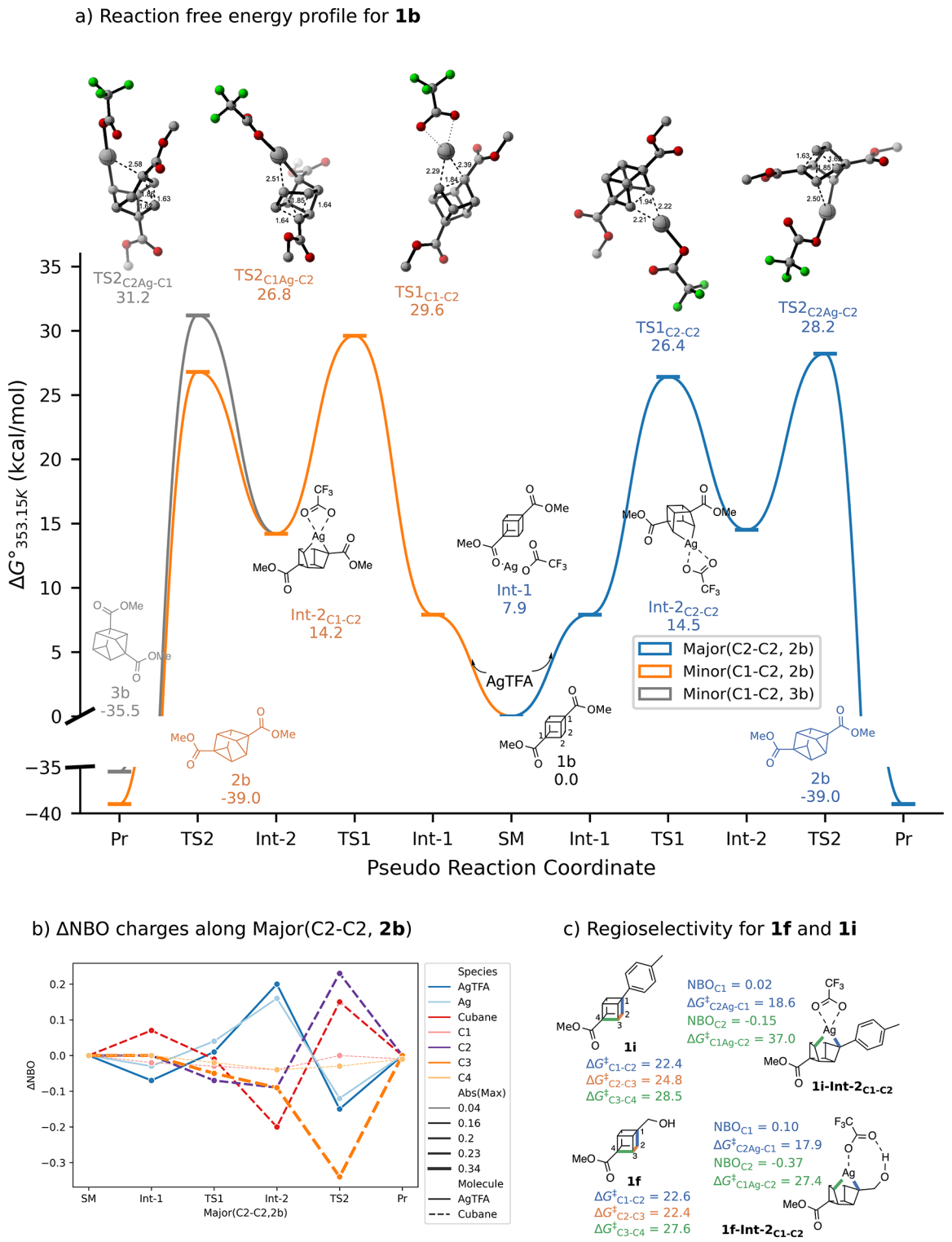

Figure 6. (a) Reaction free energy profile for isomerization of **1b** to **2b** and **3b** in kcal·mol^{-1} at 353.15 K; (b) ΔNBO graph for C1−4 and Ag atoms, as well as **1b** and AgTFA moieties for major(C2−C2, **2b**) pathway; and (c) activation free energy barriers at 313.15 K for regioselectivity determining steps for **1f** and **1i** with NBO charges in **Int-2$_{C1-C2}$**. The free energies were computed at the RPA@PBE0-D3/def2-QZVPP//PBE0-D3/def2-TZVP in toluene (COSMO-RS//COSMO) level of theory. See SI for full computational details.

pathway selectively formed the experimentally observed major product **2b** and no subsequent intermediates or branching points were located, as confirmed by dynamic reaction coordinate calculations showing the evolution of **TS2** to cuneane product **2b**. Interestingly, with substrate **1i** (see SI), a nonclassical carbocationic intermediate is found on the PES following Ag−C cleavage. From the C1−Ag−C2 intermediate, two possible cleavage pathways can take place: breaking of the Ag−C1 bond yields the minor product regioisomer **3b** ($\Delta G^{\ddagger}$ = 31.2 kcal·mol^{-1}), whereas breaking the Ag−C2 bond yields the major product **2b** ($\Delta G^{\ddagger}$ = 26.8 kcal·mol^{-1}). The mechanism for substrate **1b** isomerization thus revealed that two pathways

https://doi.org/10.1021/jacs.3c03226
J. Am. Chem. Soc. 2023, 145, 16355−16364

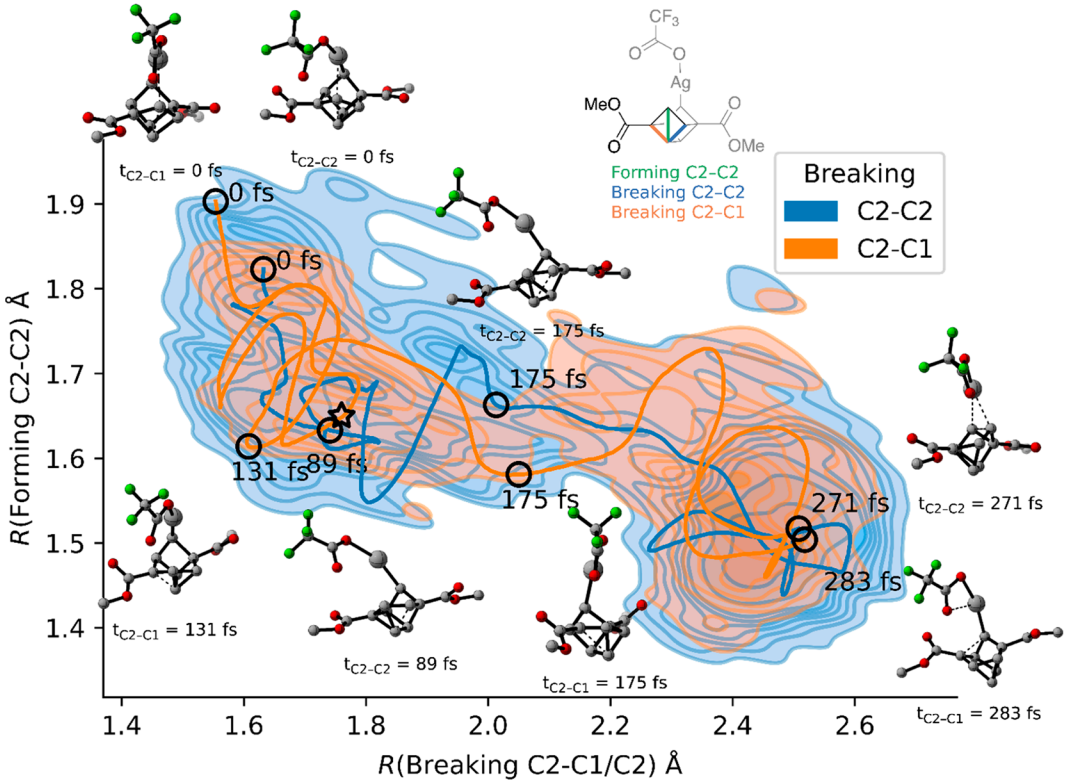

Figure 7. Plot of two representative trajectories for substrate **1b** starting at $\mathbf{TS2}_{\mathbf{C2Ag-C2}}$ (0 fs) plotted as forming the C2−C2 bond length (*y*-axis) against breaking the C2−C1 or C2−C2 bond length (*x*-axis). The blue and orange contour plots sum the 19 forward trajectories: blue for forming product **2b** (breaking the C2−C2 bond) and orange for forming product **3b** (breaking C2−C1). The blue line is a trajectory that ends at **2b** (blue area), and the orange line is a trajectory that ends at **3b** (orange area). The star indicates the position of the DFT optimized nonclassical carbocation (SI), and circles pinpoint the time of structure snapshot displayed in 3D. For full details, see SI.

contribute to the major product formation; major(C2−C2, **2b**) and minor(C1−C2, **2b**) with 88.0% and 11.9% contributions, respectively, while each of the three branches had different turnover determining steps.

To understand the regioselectivity, we analyzed NBO charges along the major(C2−C2, **2b**) reaction coordinate (Figure 6b). Compared to the substrate·AgTFA complex **Int-1**, in both $\mathbf{TS1}_{\mathbf{C2-C2}}$ and $\mathbf{Int\text{-}2}_{\mathbf{C2-C2}}$, the two carbons now attached to silver gain electron density (ΔNBO < 0), while the catalyst loses electron density. This net transfer of charge from catalyst to substrate is indicative of C−C oxidative insertion, which accounts for the lower barrier of insertion into the C2−C2 bond. Accordingly, we expect the initial insertion will generally favor more electron-rich σ_{C-C} bonds of cubane derivatives: in this case, the C1−C2 bond is less electron-rich (*α*-position of the methyl ester) and $\mathbf{TS1}_{\mathbf{C1-C2}}$ has a higher activation free energy barrier by more than 3 kcal·mol^{-1}. In the next step, *i.e.*, $\mathbf{TS2}_{\mathbf{C2Ag-C2}}$ in Figure 6b, Ag−C bond-breaking is accompanied by substantial charge separation involving the accumulation of carbocationic character at the separating carbon atom. Due to symmetry in $\mathbf{Int\text{-}2}_{\mathbf{C2-C2}}$, fragmentation of either Ag−C bond is degenerate. However, for the minor pathway, cleavage of the Ag−C2 bond is favored over Ag−C1 by more than 4 kcal·mol^{-1} since the buildup of positive charge at C1 is substantially less favorable (see Figure 6a).

We next investigated the isomerization of substrates **1i** and **1f**, which result in opposite regioselectivity to **1b**, selectively forming the 1,3-cuneane product. Oxidative addition barriers for these less electron-deficient substrates are several kcal·mol^{-1} lower than those for **1b**, with insertion preferentially occurring away from the electron-withdrawing ester group. For **1i**, addition adjacent to the aromatic ring at the C1−C2 bond is favored over the C2−C3 or C3−C4 bonds with activation free energy barriers of 22.4, 24.8, and 28.5 kcal·mol^{-1}, respectively (Figure 6c). Subsequent breaking of the Ag−C1 bond is then favored over that of the Ag−C2 bond (Figure 6c), with positive charge accumulating at the benzylic position in $\mathbf{TS2}_{\mathbf{C2Ag-C1}}$. The ensuing intermediate is a nonclassical carbocation,[44] which falls to the final 1,3-cuneane product, **3i**, with a very small barrier of 0.2 kcal·mol^{-1}.

For **1f**, C1−C2 and C2−C3 additions are nearly isoenergetic with activation free energy barriers of 22.6 and 22.4 kcal·mol^{-1}, respectively, whereas C3−C4 addition is significantly higher at 27.6 kcal·mol^{-1} (see Figure 6c). In both $\mathbf{TS1}_{\mathbf{C1-C2}}$ and $\mathbf{TS1}_{\mathbf{C2-C3}}$, the hydroxyl group of **1f** is hydrogen-bonded to the TFA oxygen, but only the C2−C3 activation free energy barrier was lowered compared to **1i**. The charge separation was even more pronounced in $\mathbf{1f\text{-}Int\text{-}2}_{\mathbf{C1-C2}}$ than in $\mathbf{1i\text{-}Int\text{-}2}_{\mathbf{C1-C2}}$ and, again, the Ag−C bond to more electropositive carbon was broken, leading to the major product **3f**. Likewise, the two carbons in $\mathbf{1f\text{-}Int\text{-}2}_{\mathbf{C2-C3}}$ demonstrated divergent polarization, C2 becoming more positive and C3 more negative, and the scission of the Ag−C2 bond was favored (see SI). Since the turnover determining step for both C1−C2 and C2−C3 bond activation was isoenergetic with **1f**, both pathways contribute almost equally to the formation of **3f**. Again, while the Ag−C bond scission in $\mathbf{TS2}_{\mathbf{C2Ag-C1}}$ can evolve to only **3f**, $\mathbf{TS2}_{\mathbf{C3Ag-C2}}$ (SI) on the other hand could potentially lead to both **2f** and **3f**, while dynamic reaction coordinate calculation connected $\mathbf{TS2}_{\mathbf{C3Ag-C2}}$ to only **3f**.

https://doi.org/10.1021/jacs.3c03226
J. Am. Chem. Soc. 2023, 145, 16355−16364

Because the static potential-energy surface indicated intermediates with significant carbocation character, nonclassical bonding (**1i-Int-3**, see SI), and possible bifurcation points (e.g., after $\mathbf{TS2}_{C2Ag-C2}$) that could lead to both major and minor products, we initiated quasiclassical direct dynamics trajectory calculations. Trajectories initiated from transition-state structures were sampled using zero-point and thermal local mode sampling at 343 K and propagated with an average time step of 0.5 fs. Figure 7 plots two representative trajectories starting at $\mathbf{TS2}_{C2Ag-C2}$ (for **1b**). One trajectory leads to **2b**, and the other, **3b**. In both trajectories a nonclassical carbocation type structure occurs close to 100 fs after the transition state, but this structure is extremely short-lived and within another 100 fs evolves to become either **2b** or **3b**, which indicates this intermediate might be best considered dynamically skipped. From 20 trajectories, only one trajectory recrossed to $\mathbf{Int\text{-}2}_{C2-C2}$, 15 ended at the major product **2b**, and four ended at the minor product **3b**. This indicates that in addition to transition state selectivity there is also dynamic selectivity; however, the transition state predicts the major product.

Thus, based on computational analysis, a set of qualitative rules could be established for the activation of 1,4-substituted cubanes. First, the initial addition favors more electron-rich C−C σ-bonds, such as those adjacent to an electron-donating group, *e.g.*, C1−C2 with substrates **1f** and **1i**, or remote from electron-withdrawing groups, like C2−C2 for **1b**. Second, the two carbons attached to silver in bridging **Int-2** exhibit charge separation if the carbons are not equivalent. Ag−C cleavage results in an accumulation of carbocationic character more favorably adjacent to an electron-donating substituent and is avoided adjacent to an electron-withdrawing group, as in $\mathbf{TS2}_{C1Ag-C2}$ and $\mathbf{TS2}_{C2Ag-C1}$. Third, at least two distinct pathways converge to form the major regioisomer. In our static studies of the PES for **1i**, a metastable nonclassical carbocation intermediate is formed by Ag−C bond breaking, with a small barrier toward cuneane formation. For **1b**, such an intermediate is skipped on the PES. However, quasi-classical dynamic trajectories indicate that a similar nonclassical carbocation occurs as a transient, dynamic intermediate, serving as a bifurcation point for products **2b** and **3b**. Thus, while transition states provide prediction of the major product the regioselectivity is partially influenced by dynamic effects.

CONCLUSIONS

In summary, we have further developed the Ag^{I}-catalyzed isomerization of cubanes to cuneanes with an emphasis on the generation of differentially 1,3-disubstituted cuneanes. We explored the mechanism of the reaction computationally and were able to develop a predictive model for the observed regioselectivity trends. We achieved several functional group interconversions on the cuneane scaffold, but its skeleton appears to make derivatives more fragile than the corresponding cubanes, despite having lower strain energy. This relative kinetic sensitivity (to a variety of conditions) may be a consequence of cuneane's embedded cyclopropane rings. Skeletal sensitivity hindered our study of energetic nitrate ester derivatives but led us to extensively characterize the analogous cubane **5f**. Despite the imperfect translation of cubane reactivity onto cuneane congeners, we hope this work will facilitate the study of cuneane derivatives, particularly differentially disubstituted species, in diverse applications.

ASSOCIATED CONTENT

Supporting Information

The Supporting Information is available free of charge at https://pubs.acs.org/doi/10.1021/jacs.3c03226.

Experimental procedures, characterization data, NMR spectra, X-ray crystallographic (PDF)

Computational details (PDF)

Accession Codes

CCDC 2113847−2113848, 2114060, 2123861−2123862, and 2215914 contain the supplementary crystallographic data for this paper. These data can be obtained free of charge via www.ccdc.cam.ac.uk/data_request/cif, or by emailing data_request@ccdc.cam.ac.uk, or by contacting The Cambridge Crystallographic Data Centre, 12 Union Road, Cambridge CB2 1EZ, UK; fax: +44 1223 336033.

AUTHOR INFORMATION

Corresponding Authors

Daniel H. Ess − *Department of Chemistry & Biochemistry, Brigham Young University, Provo, Utah 84602, United States;* orcid.org/0000-0001-5689-9762; Email: dhe@chem.byu.edu

Robert S. Paton − *Department of Chemistry, Colorado State University, Fort Collins, Colorado 80523, United States;* orcid.org/0000-0002-0104-4166; Email: robert.paton@colostate.edu

Corey R. J. Stephenson − *Department of Chemistry, University of Michigan, Ann Arbor, Michigan 48109, United States;* orcid.org/0000-0002-2443-5514; Email: crjsteph@umich.edu

Authors

Jeong-Yu Son − *Department of Chemistry, University of Michigan, Ann Arbor, Michigan 48109, United States*

Santeri Aikonen − *Department of Chemistry, Colorado State University, Fort Collins, Colorado 80523, United States;* orcid.org/0000-0003-2675-7290

Nathan Morgan − *Department of Chemistry & Biochemistry, Brigham Young University, Provo, Utah 84602, United States*

Alexander S. Harmata − *Department of Chemistry, University of Michigan, Ann Arbor, Michigan 48109, United States*

Jesse J. Sabatini − *US Army Research Laboratory, Energetics Technology Branch, Aberdeen Proving Ground, Maryland 21005, United States;* orcid.org/0000-0001-7903-8973

Rosario C. Sausa − *DEVCOM Army Research Laboratory, Energetics Simulation & Modeling Branch, Aberdeen Proving Ground, Maryland 21005, United States;* orcid.org/0000-0003-3183-0106

Edward F. C. Byrd − *DEVCOM Army Research Laboratory, Energetics Simulation & Modeling Branch, Aberdeen Proving Ground, Maryland 21005, United States*

Complete contact information is available at: https://pubs.acs.org/10.1021/jacs.3c03226

Author Contributions

#J.-Y.S. and S.A. contributed equally.

Notes

The authors declare no competing financial interest.

https://doi.org/10.1021/jacs.3c03226
J. Am. Chem. Soc. 2023, 145, 16355−16364

■ ACKNOWLEDGMENTS

The dynamics trajectories reported in this work were supported by United States National Science Foundation Chemical Structure, Dynamics, and Mechanisms B (CSDM-B) Program under Award CHE 1952420 to D.H.E. D.H.E. also acknowledges BYU's Office of Research Computing. R.S.P. acknowledges support from the NSF (CHE-1955876) and computational resources from the RMACC Summit supercomputer supported by the NSF (ACI-1532235 and ACI-1532236), the University of Colorado Boulder and Colorado State University, and XSEDE through allocation TG-CHE180056. C.R.J.S. acknowledges that research reported in this publication was supported by the National Institute of General Medical Sciences of the National Institutes of Health under Award Number R35-GM144286 and the University of Michigan. This material is based upon work supported by the National Science Foundation Graduate Research Fellowship under Grant No. (DGE 1841052) (for A.S.H.). Funding from the US Army is gratefully acknowledged.

■ ABBREVIATIONS

AgTFA, silver(I) trifluoroacetate; FGI, functional group interconversion; NHPI, phthalimide *N*-oxyl group; EDC, 1-Ethyl-3-(3-(dimethylamino)propyl)carbodiimide hydrochloride; DMAP, dimethylaminopyridine

■ REFERENCES

(1) Eaton, P. E.; Cole, T. W. The Cubane System. *J. Am. Chem. Soc.* **1964**, *86* (5), 962−964.
(2) Eaton, P. E.; Zhang, M.-X. Octanitrocubane: A New Nitrocarbon. *Propellants, Explosive, Pyrotechnics* **2002**, *27*, 1−6.
(3) Eaton, P. E. Cubanes: Starting Materials for the Chemistry of the 1990s and the New Century. *Angewandte Chemie International Edition in English* **1992**, *31* (11), 1421−1436.
(4) Chalmers, B. A.; Xing, H.; Houston, S.; Clark, C.; Ghassabian, S.; Kuo, A.; Cao, B.; Reitsma, A.; Murray, C. E. P.; Stok, J. E.; Boyle, G. M.; Pierce, C. J.; Littler, S. W.; Winkler, D. A.; Bernhardt, P. V.; Pasay, C.; De Voss, J. J.; McCarthy, J.; Parsons, P. G.; Walter, G. H.; Smith, M. T.; Cooper, H. M.; Nilsson, S. K.; Tsanaktsidis, J.; Savage, G. P.; Williams, C. M. Validating Eaton's Hypothesis: Cubane as a Benzene Bioisostere. *Angew. Chem., Int. Ed.* **2016**, *55* (11), 3580−3585.
(5) Al-Janabi, A.; Mandle, R. J. Utilising Saturated Hydrocarbon Isosteres of para Benzene in the Design of Twist-Bend Nematic Liquid Crystals. *ChemPhysChem* **2020**, *21* (8), 697−701.
(6) Bényei, G.; Jalsovszky, I.; Demus, D.; Prasad, K.; Rao, S.; Vajda, A.; Jákli, A.; Fodor-Csorba, K. First liquid crystalline cuneane-caged derivatives: a structure−property relationship study. *Liq. Cryst.* **2006**, *33* (6), 689−696.
(7) Eaton, P. E.; Cassar, L.; Halpern, J. Silver(I)- and palladium(II)-catalyzed isomerizations of cubane. Synthesis and characterization of cuneane. *J. Am. Chem. Soc.* **1970**, *92* (21), 6366−6368.
(8) (a) Cassar, L.; Eaton, P. E.; Halpern, J. Catalysis of symmetry-restricted reactions by transition metal compounds. Valence isomerization of cubane. *J. Am. Chem. Soc.* **1970**, *92*, 3515−3518. (b) Houston, S. D.; Xing, H.; Bernhardt, P. V.; Vanden Berg, T. J.; Tsanaktsidis, J.; Savage, G. P.; Williams, C. M. Cyclooctatetraenes through Valence Isomerization of Cubanes: Scope and Limitations. *Chemistry − A European Journal* **2019**, *25* (11), 2735−2739.
(9) (a) Takebe, H.; Matsubara, S. Catalytic Asymmetric Synthesis of 2,6-Disubstituted Cuneanes through Enantioselective Constitutional Isomerization of 1,4-Disubstituted Cubanes. *Eur. J. Org. Chem.* **2022**, *2022*, e202200567. (b) Smith, E.; O'Brien, L.; Jones, K.; Argent, S.; Salome, C.; Lefebvre, Q.; Valery, A.; Newton, G.; Lam, H. W. Silver (I)-Catalyzed Synthesis of Cuneanes from Cubanes and their Investigation as Isosteres. *ChemRxiv* **2023**, DOI: 10.26434/chemrxiv-2023-l8q0t, This content is a preprint and has not been peer-reviewed. We coordinated submission with the authors to the Journal of the American Chemical Society, and the peer-reviewed manuscript can be found at DOI: 10.1021/jacs.3c03207.. (c) Following submission of this manuscript, an additional preprint was released describing the synthesis of 1,3-disubstituted cuneanes, showing selectivity trends consistent with those we have observed. Nagasawa, S.; Fujiwara, K.; Maeyama, R.; Segawa, R.; Hirasawa, N.; Iwabuchi, Y. Selective Synthesis of 1,3-Substituted Cuneanes: En Route to Potent Bioisosteres of m-Substituted Benzenes. *ChemRxiv* **2023**, DOI: 10.26434/chemrxiv-2023-fgxxm, This content is a preprint and has not been peer-reviewed..
(10) For information pertaining to the synthesis of saturated isosteres of benzenes, particularly *meta*-disubstituted benzenes, and recent examples thereof: (a) Mykhailiuk, P. K. Saturated bioisosteres of benzene: where to go next? *Organic & Biomolecular Chemistry* **2019**, *17* (11), 2839−2849. (b) Iida, T.; Kanazawa, J.; Matsunaga, T.; Miyamoto, K.; Hirano, K.; Uchiyama, M. Practical and Facile Access to Bicyclo[3.1.1]heptanes: Potent Bioisosteres of *meta*-Substituted Benzenes. *J. Am. Chem. Soc.* **2022**, *144*, 21848−21852. (c) Frank, N.; Nugent, J.; Shire, B. R.; Pickford, H. D.; Rabe, P.; Sterling, A. J.; Zarganes-Tzitzikas, T.; Grimes, T.; Thompson, A. L.; Smith, R. C.; Schofield, C. J.; Brennan, P. E.; Duarte, F.; Anderson, E. A. Synthesis of *meta*-substituted arene bioisosteres from [3.1.1]propellane. *Nature* **2022**, *611*, 721−726. (d) Wiesenfeldt, M. P.; Rossi-Ashton, J. A.; Perry, I. B.; Diesel, J.; Garry, O. L.; Bartels, F.; Coote, S. C.; Ma, X.; Yeung, C. S.; Bennett, D. J.; MacMillan, D. W. C. General access to cubanes as benzene bioisosteres. *Nature* **2023**, *618*, 513−518. (e) Epplin, R. C.; Paul, S.; Herter, L.; Salome, C.; Hancock, E. N.; Larrow, J. F.; Baum, E. W.; Dunstan, D. R.; Ginsburg-Moraff, C.; Fessard, T. C.; Brown, M. K. [2]-Ladderanes as isosteres for meta-substituted aromatic rings and rigidified cyclohexanes. *Nat. Commun.* **2022**, *13*, 6056.
(11) Kirmse, W.; Sandkühler, P. Synthese und Umlagerung 1-substituierter Bicyclo[2.2.0]hexane. *Liebigs Annalen der Chemie* **1981**, *1981* (8), 1394−1406.
(12) Okude, R.; Mori, G.; Yagi, A.; Itami, K. Programmable synthesis of multiply arylated cubanes through C−H metalation and arylation. *Chemical Science* **2020**, *11* (29), 7672−7675.
(13) Qin, T.; Malins, L. R.; Edwards, J. T.; Merchant, R. R.; Novak, A. J. E.; Zhong, J. Z.; Mills, R. B.; Yan, M.; Yuan, C.; Eastgate, M. D.; Baran, P. S. Nickel-Catalyzed Barton Decarboxylation and Giese Reactions: A Practical Take on Classic Transforms. *Angew. Chem., Int. Ed.* **2017**, *56* (1), 260−265.
(14) Dubikhin, V. V.; Prokudin, V. G.; Nazina, L. D.; Romanova, L. B.; Eremenko, L. T.; Nazin, G. M. Kinetics and mechanism of the thermal decomposition of 1-bromo-4-nitroxymethylcubane. *Kinetics and Catalysis* **2007**, *48*, 345−347.
(15) Romanova, L. B.; Barinova, L. S.; Zakharov, V. V.; Eremenko, L. T.; Aleksandrov, G. G.; Eremenko, I. L. Cubane derivatives 10. Synthesis and molecular structures of nitroxymethylcubanes. *Russian Chemical Bulletin* **2010**, *59*, 1051−1055.
(16) Nesterenko, D. A.; Garanin, V. A.; Kazakov, A. I.; Korepin, A. G.; Romanova, L. B. Energetic properties and impact sensitivity of crystalline explosives. *Russian Journal of Physical Chemistry B* **2014**, *8*, 701−711.
(17) Lempert, D. B.; Zyuzin, I. N.; Averkov, I. S.; Raznoschikov, V. V.; Yanovskii, L. S. Some Cubane Derivatives as Potential Components of Solid Gas Generator Propellants. *Russian Journal of Applied Chemistry* **2021**, *94*, 172−181.
(18) Lal, S.; Bhattacharjee, A.; Chowdhury, A.; Kumbhakarna, N.; Namboothiri, I. N. N. Approaches to 1,4-Disubstituted Cubane Derivatives as Energetic Materials: Design, Theoretical Studies and Synthesis. *Chem.—Asian J.* **2022**, *17*, No. e2022004.
(19) NATO Standardization Agreement (STANAG) on Explosives, Friction Sensitivity Tests, No. 4487, 1st ed., August 22, 2002.
(20) NATO Standardization Agreement (STANAG) on Explosives, Impact Sensitivity Tests, No. 4489, 1st ed., September 17, 1999.

(21) Balasubramani, S. G.; Chen, G. P.; Coriani, S.; Diedenhofen, M.; Frank, M. S.; Franzke, Y. J.; Furche, F.; Grotjahn, R.; Harding, M. E.; Hättig, C.; Hellweg, A.; Helmich-Paris, B.; Holzer, C.; Huniar, U.; Kaupp, M.; Khah, A. M.; Khani, S. K.; Müller, T.; Mack, F.; Nguyen, B. D.; Parker, S. M.; Perlt, E.; Rappoport, D.; Reiter, K.; Roy, S.; Rückert, M.; Schmitz, G.; Sierka, M.; Tapavicza, E.; Tew, D. P.; van Wüllen, C. v.; Voora, V. K.; Weigend, F.; Wodyński, A.; Yu, J. M. TURBOMOLE: Modular program suite for ab initio quantum-chemical and condensed-matter simulations. *J. Chem. Phys.* **2020**, *152* (18), No. 184107.
(22) Neese, F. Software update: the ORCA program system, version 4.0. *WIREs Comput. Mol. Sci.* **2018**, *8* (1), No. e1327.
(23) Grimme, S.; Bannwarth, C.; Shushkov, P. A Robust and Accurate Tight-Binding Quantum Chemical Method for Structures, Vibrational Frequencies, and Noncovalent Interactions of Large Molecular Systems Parametrized for All spd-Block Elements (Z = 1−86). *J. Chem. Theory Comput.* **2017**, *13* (5), 1989−2009.
(24) Pracht, P.; Bohle, F.; Grimme, S. Automated exploration of the low-energy chemical space with fast quantum chemical methods. *Phys. Chem. Chem. Phys.* **2020**, *22* (14), 7169−7192.
(25) Grimme, S.; Bohle, F.; Hansen, A.; Pracht, P.; Spicher, S.; Stahn, M. Efficient Quantum Chemical Calculation of Structure Ensembles and Free Energies for Nonrigid Molecules. *J. Phys. Chem. A* **2021**, *125* (19), 4039−4054.
(26) Adamo, C.; Barone, V. Toward reliable density functional methods without adjustable parameters: The PBE0 model. *J. Chem. Phys.* **1999**, *110* (13), 6158−6170.
(27) Grimme, S.; Antony, J.; Ehrlich, S.; Krieg, H. A consistent and accurate ab initio parametrization of density functional dispersion correction (DFT-D) for the 94 elements H-Pu. *J. Chem. Phys.* **2010**, *132* (15), No. 154104.
(28) Weigend, F.; Ahlrichs, R. Balanced basis sets of split valence, triple zeta valence and quadruple zeta valence quality for H to Rn: Design and assessment of accuracy. *Phys. Chem. Chem. Phys.* **2005**, *7* (18), 3297−3305.
(29) Bühl, M.; Reimann, C.; Pantazis, D. A.; Bredow, T.; Neese, F. Geometries of Third-Row Transition-Metal Complexes from Density-Functional Theory. *J. Chem. Theory Comput.* **2008**, *4* (9), 1449−1459.
(30) Waller, M. P.; Braun, H.; Hojdis, N.; Bühl, M. Geometries of Second-Row Transition-Metal Complexes from Density-Functional Theory. *J. Chem. Theory Comput.* **2007**, *3* (6), 2234−2242.
(31) Cramer, C. J.; Truhlar, D. G. Density functional theory for transition metals and transition metal chemistry. *Phys. Chem. Chem. Phys.* **2009**, *11* (46), 10757−10816.
(32) Chen, G. P.; Voora, V. K.; Agee, M. M.; Balasubramani, S. G.; Furche, F. Random-Phase Approximation Methods. *Annu. Rev. Phys. Chem.* **2017**, *68* (1), 421−445.
(33) Klamt, A. The COSMO and COSMO-RS solvation models. *WIREs Comput. Mol. Sci.* **2018**, *8* (1), No. e1338.
(34) Schäfer, A.; Klamt, A.; Sattel, D.; Lohrenz, J. C. W.; Eckert, F. COSMO Implementation in TURBOMOLE: Extension of an efficient quantum chemical code towards liquid systems. *Phys. Chem. Chem. Phys.* **2000**, *2* (10), 2187−2193.
(35) Klamt, A.; Schüürmann, G. COSMO: a new approach to dielectric screening in solvents with explicit expressions for the screening energy and its gradient. *Journal of the Chemical Society, Perkin Transactions 2* **1993**, No. 5, 799−805.
(36) Klamt, A. *COSMOtherm, 19*; COSMOlogic GmbH & Co. KG, a Dassault Systèmes company: 2019.
(37) Klamt, A.; Jonas, V.; Bürger, T.; Lohrenz, J. C. W. Refinement and Parametrization of COSMO-RS. *J. Phys. Chem. A* **1998**, *102* (26), 5074−5085.
(38) Klamt, A. Conductor-like Screening Model for Real Solvents: A New Approach to the Quantitative Calculation of Solvation Phenomena. *J. Phys. Chem.* **1995**, *99* (7), 2224−2235.
(39) Grimme, S. Supramolecular Binding Thermodynamics by Dispersion-Corrected Density Functional Theory. *Chem.—Eur. J.* **2012**, *18* (32), 9955−9964.
(40) Frisch, M. J.; Trucks, G. W.; Schlegel, H. B.; Scuseria, G. E.; Robb, M. A.; Cheeseman, J. R.; Scalmani, G.; Barone, V.; Petersson, G. A.; Nakatsuji, H.; Li, X.; Caricato, M.; Marenich, A. V.; Bloino, J.; Janesko, B. G.; Gomperts, R.; Mennucci, B.; Hratchian, H. P.; Ortiz, J. V.; Izmaylov, A. F.; Sonnenberg, J. L.; Williams; Ding, F.; Lipparini, F.; Egidi, F.; Goings, J.; Peng, B.; Petrone, A.; Henderson, T.; Ranasinghe, D.; Zakrzewski, V. G.; Gao, J.; Rega, N.; Zheng, G.; Liang, W.; Hada, M.; Ehara, M.; Toyota, K.; Fukuda, R.; Hasegawa, J.; Ishida, M.; Nakajima, T.; Honda, Y.; Kitao, O.; Nakai, H.; Vreven, T.; Throssell, K.; Montgomery, J. A., Jr.; Peralta, J. E.; Ogliaro, F.; Bearpark, M. J.; Heyd, J. J.; Brothers, E. N.; Kudin, K. N.; Staroverov, V. N.; Keith, T. A.; Kobayashi, R.; Normand, J.; Raghavachari, K.; Rendell, A. P.; Burant, J. C.; Iyengar, S. S.; Tomasi, J.; Cossi, M.; Millam, J. M.; Klene, M.; Adamo, C.; Cammi, R.; Ochterski, J. W.; Martin, R. L.; Morokuma, K.; Farkas, O.; Foresman, J. B.; Fox, D. J. *Gaussian 16*, Rev. C.01; Gaussian Inc.: Wallingford, CT, 2016.
(41) Paquette, L. A.; Beckley, R. S.; Farnham, W. B. Silver(I) ion catalyzed rearrangements of strained. sigma. bonds. XXVII. Kinetic analysis of the silver(I)-catalyzed 1,8-bishomocubane-snoutane rearrangement. *J. Am. Chem. Soc.* **1975**, *97* (5), 1089−1100.
(42) Bishop, K. C. Transition metal catalyzed rearrangements of small ring organic molecules. *Chem. Rev.* **1976**, *76* (4), 461−486.
(43) Elkoush, T.; Reich, N. D.; Campbell, M. G. Dinuclear Silver Complexes in Catalysis. *Angew. Chem., Int. Ed. Engl.* **2021**, *60* (42), 22614−22622.
(44) Scholz, F.; Himmel, D.; Heinemann, F. W.; Schleyer, P. v. R.; Meyer, K.; Krossing, I. Crystal Structure Determination of the Nonclassical 2-Norbornyl Cation. *Science* **2013**, *341* (6141), 62−64.

https://doi.org/10.1021/jacs.3c03226
J. Am. Chem. Soc. 2023, 145, 16355−16364